SAND2020-0052R

Sandia National Laboratories

Operated for the United States Department of Energy
by National Technology and Engineering Solutions
of Sandia, LLC.

Albuquerque, New Mexico 87185-0101
Livermore, California 94551-0969

date: November 26th, 2018

to:
Bryan Tebay Org 2444 MS 0451
Ryland Hubka Org 2444 MS 0451
Walter Kruse Org 2444 MS 0451

from:
Wen Dong Org 1864 MS 0889
Pin Yang Org 1816 MS 0958

subject: Effect of thermal expansion in PZT/Stainless Steel bilayer disk

The purpose of this memo is to analytically investigate the possible effects of thermal expansion on the electromechanical properties of the Sumida Components GmbH piezoelectric composite disk followed by experimental verification. Linear electromechanical, electrothermal, and thermomechanical constitutive law is assumed.

The geometry of the piezoelectric composite disk is comprised of a circular layer of poled piezoelectric PZT5A with thickness 0.12mm and diameter 9mm bonded concentrically on a stainless-steel layer of thickness 0.10mm and diameter 10.6mm as shown in Figure 1.a. The design of the piezoelectric composite disk includes a permissible convex deflection of 0.06mm at room temperature as shown in Figure 1.b. It is believed that the disk curvature is an intentional feature as the primary mode of electromechanical excitation is induced by disk flexing. Flex caused by pressure applied on top of the disk causes change to the in-plane stress and leads to 3-1 mode electromechanical excitation in the PZT.

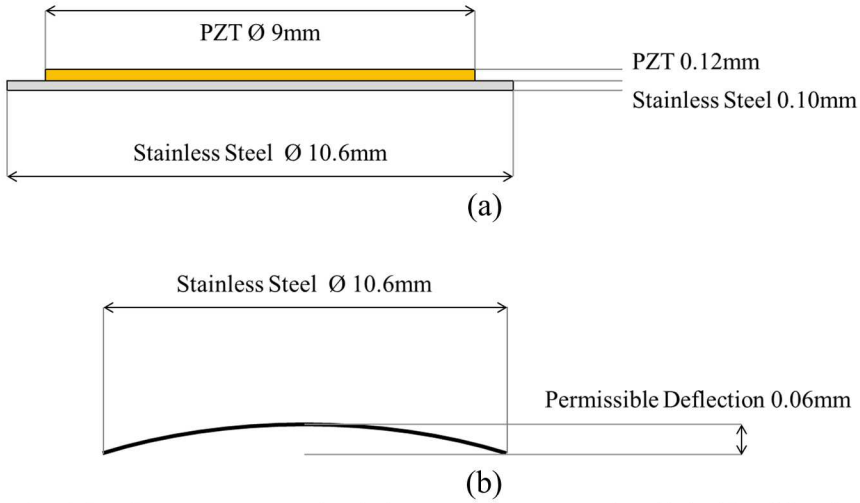

Figure 1. a) Side view of PZT5A/stainless-steel composite disk. b) Side view of permissible convex deflection in piezoelectric composite disk at room temperature.

CLASSICAL PLATE/LAMINATE THEORY

Kinematics

In the classical Kirchoff-Love plate/laminate theory approach, it is assumed that there is perfect adhesion between the PZT and stainless-steel layers, normals to the mid surface remain normal, the thickness of the plate does not change, and the stress state is plane-stress. The resulting total strain field $\boldsymbol{\varepsilon}$ is as shown in Equation (1) where u^0, v^0, and w^0 are the composite plate's mid plane displacement s in the in plane x and y and out of plane z axes. $\boldsymbol{\varepsilon}^0$ and $\boldsymbol{\kappa}$ are the mid plane in plane stresses and mid plane curvatures respectively. The strain state is assumed to be uniform in plane and varies only with thickness.

$$\begin{aligned}\begin{Bmatrix}\varepsilon_x(z)\\ \varepsilon_y(z)\\ \gamma_{xy}(z)\end{Bmatrix}^{Total} &= \begin{Bmatrix}\varepsilon_x^0\\ \varepsilon_y^0\\ \gamma_{xy}^0\end{Bmatrix} + z\begin{Bmatrix}\kappa_x\\ \kappa_y\\ 2\kappa_{xy}\end{Bmatrix}\\ &= \begin{Bmatrix}\dfrac{du^0}{dx}\\ \dfrac{dv^0}{dy}\\ \dfrac{du^0}{dy}+\dfrac{dv^0}{dx}\end{Bmatrix} - z\begin{Bmatrix}\dfrac{d^2w^0}{dx^2}\\ \dfrac{d^2w^0}{dy^2}\\ 2\dfrac{d^2w^0}{dxdy}\end{Bmatrix}\end{aligned} \tag{1}$$

Constitutive

Isotropic constitutive relations can be assumed for both the PZT5A and stainless-steel layers as the PZT5A has roughly transverse isotropic properties along the direction of polarization and the polarization direction is in the out of plane z axis. This simplifies the constitutive relation of the k th layer such that the stress field $\boldsymbol{\sigma}$ is as shown in Equation (2).

$$\begin{Bmatrix} \sigma_x(z) \\ \sigma_y(z) \\ \tau_{xy}(z) \end{Bmatrix}_k = \begin{bmatrix} C_{11} & C_{12} & 0 \\ C_{12} & C_{11} & 0 \\ 0 & 0 & C_{66} \end{bmatrix}_k \begin{Bmatrix} \varepsilon_x(z) \\ \varepsilon_y(z) \\ \gamma_{xy}(z) \end{Bmatrix}_k^{Elastic} \tag{2}$$

The constitutive relationship between the total strain, elastic strain, piezoelectric strain, and thermal strain is as shown in Equation (3) for open circuit (OC) and short circuit (SC) systems where either the electric displacement or electric field is held constant. **s**, **d**, **g**, **k**, $\boldsymbol{\beta}$, $\boldsymbol{\alpha}$ and **p** are respectively, the compliance, stress-charge piezoelectric, stress-voltage piezoelectric, permittivity, inverse permittivity, thermal expansion, and pyroelectric coefficient tensors. **E**, **D**, T, $\boldsymbol{\sigma}$, and $\boldsymbol{\varepsilon}$ are the electric field, electric displacement, temperature, stress, and strain. Bold indicates tensor and the superscripts on coefficients indicate the superscript quantities are held constant when the coefficients are measured. Stress and strain matrices are simplified to plain-stress 2-D expressions in the plane of the composite layers.

$$\begin{aligned} \boldsymbol{\varepsilon}^{SC} &= \mathbf{s}^{ET}\boldsymbol{\sigma} + \left[\mathbf{d}^T\right]^t \mathbf{E} + \boldsymbol{\alpha}^{\sigma E}\Delta T \\ \mathbf{D} &= \mathbf{d}^T\boldsymbol{\sigma} + \mathbf{k}^{\sigma T}\mathbf{E} + \mathbf{p}^{\sigma E}\Delta T \end{aligned}$$

$$\begin{aligned} \boldsymbol{\varepsilon}^{OC} &= \underbrace{\left[\mathbf{s}^{ET} - \left[\mathbf{d}^T\right]^t \boldsymbol{\beta}^{\sigma T}\mathbf{d}^T\right]}_{\mathbf{s}^{DT}}\boldsymbol{\sigma} + \underbrace{\left[\mathbf{d}^T\right]^t \boldsymbol{\beta}^{\sigma T}}_{\left[\mathbf{g}^T\right]^t}\mathbf{D} + \underbrace{\left[\boldsymbol{\alpha}^E - \left[\mathbf{d}^T\right]^t \boldsymbol{\beta}^{\sigma T}\mathbf{p}^{\sigma E}\right]}_{\boldsymbol{\alpha}^{\sigma D}}\Delta T \\ \mathbf{E} &= -\underbrace{\boldsymbol{\beta}^{\sigma T}\mathbf{d}}_{\mathbf{g}^T}\boldsymbol{\sigma} + \boldsymbol{\beta}^{\sigma T}\mathbf{D} - \boldsymbol{\beta}^{\sigma T}\mathbf{p}^{\sigma E}\Delta T \\ \boldsymbol{\beta}^{\sigma T} &= \left[\mathbf{k}^{\sigma T}\right]^{-1} \end{aligned} \tag{3}$$

The in the open and short circuit scenarios, **D** or **E** are respectively held to zero which simplifies Equation (3) to Equation (4)

$$\begin{aligned} \boldsymbol{\varepsilon}^{SC} &= \underbrace{\mathbf{s}^{ET}\boldsymbol{\sigma}}_{Elastic} + \underbrace{\boldsymbol{\alpha}^{\sigma E}\Delta T}_{Thermal} \\ \boldsymbol{\varepsilon}^{OC} &= \underbrace{\mathbf{s}^{DT}\boldsymbol{\sigma}}_{Elastic} + \underbrace{\boldsymbol{\alpha}^{\sigma D}\Delta T}_{Thermal} \end{aligned} \tag{4}$$

Combining Equations (2) and (4), the constitutive relation for each layer k th layer is shown in Equation (5).

$$\begin{aligned}\begin{Bmatrix}\sigma_x(z)\\ \sigma_y(z)\\ \tau_{xy}(z)\end{Bmatrix}_k &= \begin{bmatrix}C_{11} & C_{12} & 0\\ C_{12} & C_{11} & 0\\ 0 & 0 & C_{66}\end{bmatrix}_k \left[\begin{Bmatrix}\varepsilon_x(z)\\ \varepsilon_y(z)\\ \gamma_{xy}(z)\end{Bmatrix}_k^{Total} - \begin{Bmatrix}\varepsilon_x\\ \varepsilon_y\\ \gamma_{xy}\end{Bmatrix}_k^{Thermal}\right]\\ &= \begin{bmatrix}C_{11} & C_{12} & 0\\ C_{12} & C_{11} & 0\\ 0 & 0 & C_{66}\end{bmatrix}_k \left[\begin{Bmatrix}\varepsilon_x^0\\ \varepsilon_y^0\\ \gamma_{xy}^0\end{Bmatrix} + z\begin{Bmatrix}\kappa_x\\ \kappa_y\\ 2\kappa_{xy}\end{Bmatrix} - \begin{Bmatrix}\alpha_1\\ \alpha_2\\ \alpha_6\end{Bmatrix}_k \Delta T\right]\end{aligned} \tag{5}$$

Resultants

Calculations of the force and moment resultants allow for the analysis of the entire composite behavior. The expressions for the force $\mathbf{N}$ and moment $\mathbf{M}$ resultants are shown in Equation (6).

$$\begin{aligned}\begin{Bmatrix}N_x\\ N_y\\ N_{xy}\end{Bmatrix} &= \int \begin{Bmatrix}\sigma_x(z)\\ \sigma_y(z)\\ \tau_{xy}(z)\end{Bmatrix} dz\\ \begin{Bmatrix}M_x\\ M_y\\ M_{xy}\end{Bmatrix} &= \int \begin{Bmatrix}\sigma_x(z)\\ \sigma_y(z)\\ \tau_{xy}(z)\end{Bmatrix} z dz\end{aligned} \tag{6}$$

Substituting Equation (5) into (6), the expression for the resultants becomes as shown in Equation (7) where z_k and z_{k-1} are the material boundary displacements from the composite midpoint.

$$\begin{aligned}\begin{Bmatrix}N_x\\ N_y\\ N_{xy}\end{Bmatrix} &= \sum_{k=1}^{N} \begin{bmatrix}C_{11} & C_{12} & 0\\ C_{12} & C_{11} & 0\\ 0 & 0 & C_{66}\end{bmatrix}_k \left[\begin{Bmatrix}\varepsilon_x^0\\ \varepsilon_y^0\\ \gamma_{xy}^0\end{Bmatrix} \int_{z_{k-1}}^{z_k} dz + \begin{Bmatrix}\kappa_x\\ \kappa_y\\ 2\kappa_{xy}\end{Bmatrix} \int_{z_{k-1}}^{z_k} z dz - \begin{Bmatrix}\alpha_1\\ \alpha_2\\ \alpha_6\end{Bmatrix}_k \Delta T \int_{z_{k-1}}^{z_k} dz\right]\\ \begin{Bmatrix}M_x\\ M_y\\ M_{xy}\end{Bmatrix} &= \sum_{k=1}^{N} \begin{bmatrix}C_{11} & C_{12} & 0\\ C_{12} & C_{11} & 0\\ 0 & 0 & C_{66}\end{bmatrix}_k \left[\begin{Bmatrix}\varepsilon_x^0\\ \varepsilon_y^0\\ \gamma_{xy}^0\end{Bmatrix} \int_{z_{k-1}}^{z_k} z dz + \begin{Bmatrix}\kappa_x\\ \kappa_y\\ 2\kappa_{xy}\end{Bmatrix} \int_{z_{k-1}}^{z_k} z^2 dz - \begin{Bmatrix}\alpha_1\\ \alpha_2\\ \alpha_6\end{Bmatrix}_k \Delta T \int_{z_{k-1}}^{z_k} z dz\right]\end{aligned} \tag{7}$$

The solution to Equation (7) is shown in Equation (8) where the ABBD matrix is the resultant stiffness matrix for the composite.

$$\begin{Bmatrix} \mathbf{N} \\ \mathbf{M} \end{Bmatrix} + \begin{Bmatrix} \mathbf{N}^{Thermal} \\ \mathbf{M}^{Thermal} \end{Bmatrix} = \begin{Bmatrix} \mathbf{N} \\ \mathbf{M} \end{Bmatrix} + \begin{Bmatrix} \mathbf{n}^{Thermal} \\ \mathbf{m}^{Thermal} \end{Bmatrix} \Delta T = \begin{bmatrix} \mathbf{A} & \mathbf{B} \\ \mathbf{B} & \mathbf{D} \end{bmatrix} \begin{Bmatrix} \boldsymbol{\varepsilon}^0 \\ \boldsymbol{\kappa} \end{Bmatrix}$$

$$\boldsymbol{\varepsilon}^0 = \begin{Bmatrix} \varepsilon_x^0 \\ \varepsilon_y^0 \\ \gamma_{xy}^0 \end{Bmatrix} \quad \boldsymbol{\kappa} = \begin{Bmatrix} \kappa_x \\ \kappa_y \\ 2\kappa_{xy} \end{Bmatrix}$$

$$\mathbf{A} = \sum_{k=1}^{N} \begin{bmatrix} C_{11} & C_{12} & 0 \\ C_{12} & C_{11} & 0 \\ 0 & 0 & C_{66} \end{bmatrix}_k \left[z_k - z_{k-1} \right]$$

$$\mathbf{B} = \sum_{k=1}^{N} \begin{bmatrix} C_{11} & C_{12} & 0 \\ C_{12} & C_{11} & 0 \\ 0 & 0 & C_{66} \end{bmatrix}_k \frac{1}{2} \left[z_k^2 - z_{k-1}^2 \right]$$

$$\mathbf{D} = \sum_{k=1}^{N} \begin{bmatrix} C_{11} & C_{12} & 0 \\ C_{12} & C_{11} & 0 \\ 0 & 0 & C_{66} \end{bmatrix}_k \frac{1}{3} \left[z_k^3 - z_{k-1}^3 \right]$$

$$\mathbf{N}^{Thermal} = \mathbf{n}^{Thermal} \Delta T = \sum_{k=1}^{N} \begin{bmatrix} C_{11} & C_{12} & 0 \\ C_{12} & C_{11} & 0 \\ 0 & 0 & C_{66} \end{bmatrix}_k \begin{Bmatrix} \alpha_1 \\ \alpha_2 \\ \alpha_6 \end{Bmatrix}_k \left[z_k - z_{k-1} \right] \Delta T \tag{8}$$

$$\mathbf{M}^{Thermal} = \mathbf{m}^{Thermal} \Delta T = \sum_{k=1}^{N} \begin{bmatrix} C_{11} & C_{12} & 0 \\ C_{12} & C_{11} & 0 \\ 0 & 0 & C_{66} \end{bmatrix}_k \begin{Bmatrix} \alpha_1 \\ \alpha_2 \\ \alpha_6 \end{Bmatrix}_k \frac{1}{2} \left[z_k^2 - z_{k-1}^2 \right] \Delta T$$

The inverse composite constitutive relationship is shown as shown in Equation (9).

$$\begin{Bmatrix} \boldsymbol{\varepsilon}^0 \\ \boldsymbol{\kappa} \end{Bmatrix} = \begin{bmatrix} \mathbf{a} & \mathbf{b} \\ \mathbf{b} & \mathbf{d} \end{bmatrix} \left[\begin{Bmatrix} \mathbf{N} \\ \mathbf{M} \end{Bmatrix} + \begin{Bmatrix} \mathbf{n}^{Thermal} \\ \mathbf{m}^{Thermal} \end{Bmatrix} \Delta T \right]$$

$$\begin{bmatrix} \mathbf{a} & \mathbf{b} \\ \mathbf{b} & \mathbf{d} \end{bmatrix} = \begin{bmatrix} \mathbf{A} & \mathbf{B} \\ \mathbf{B} & \mathbf{D} \end{bmatrix}^{-1}$$

$$\mathbf{a} = \mathbf{A}^{-1} - \left[-\mathbf{A}^{-1}\mathbf{B} \left[\mathbf{D} - \mathbf{B}\mathbf{A}^{-1}\mathbf{B} \right]^{-1} \mathbf{B}\mathbf{A}^{-1} \right] \tag{9}$$

$$\mathbf{b} = -\mathbf{A}^{-1}\mathbf{B} \left[\mathbf{D} - \mathbf{B}\mathbf{A}^{-1}\mathbf{B} \right]^{-1}$$

$$\mathbf{d} = \left[\mathbf{D} - \mathbf{B}\mathbf{A}^{-1}\mathbf{B} \right]^{-1}$$

APPLICATION TO PZT COMPOSITE DISK

Material Parameters

The grade of stainless-steel is not specified in the Sumida Components GmbH drawings. Parameters for AISI 302 stainless-steel were taken from (http://asm.matweb.com/search/SpecificMaterial.asp?bassnum=mq304a and https://www.engineeringtoolbox.com/thermal-expansion-metals-d_859.html) and replicated below.

$$
\begin{aligned}
E &= 180\left\langle \times 10^{9}\, Pa \right\rangle \\
\nu &= 0.29 \\
\begin{bmatrix} C_{11} & C_{12} & 0 \\ C_{12} & C_{11} & 0 \\ 0 & 0 & C_{66} \end{bmatrix}_{SS316L} &= \begin{bmatrix} 196.53 & 56.99 & 0 \\ 56.99 & 196.53 & 0 \\ 0 & 0 & 69.78 \end{bmatrix} \left\langle \times 10^{9}\, Pa \right\rangle \\
\begin{Bmatrix} \alpha_1 \\ \alpha_2 \\ \alpha_6 \end{Bmatrix}_{SS316L} &= \begin{Bmatrix} 9.0 \\ 9.0 \\ 0 \end{Bmatrix} \left\langle \times 10^{-6} \frac{1}{K} \right\rangle
\end{aligned}
\tag{10}
$$

The elastic, piezoelectric, and permittivity parameters for generic PZT5A are acquired from (http://www.efunda.com/materials/piezo/material_data/matdata_output.cfm?Material_ID=PZT-5A) and thermal expansion and pyroelectric coefficients are from Morgan Ceramics TP226. $\grave{o}_{33}$ permittivity values are calculated from measured capacitance values in shown in Table 1. The values are reproduced below.

Table 1. Measured capacitance and permittivity values of composite disks.

Frequency (Hz)	Capacitance (nF) Specimen 1	Specimen 2	Specimen 3	Average	Permittivity $\grave{o}_{33}$ ($\grave{o}_0$)
40	9.41	9.18	9.27	9.29	1979
100	9.35	9.20	9.26	9.27	1975
1000	9.13	9.13	9.16	9.14	1947

$$
\begin{bmatrix} S_{11} & S_{12} & 0 \\ S_{12} & S_{11} & 0 \\ 0 & 0 & S_{66} \end{bmatrix}_{PZT5A}^{ET} = \begin{bmatrix} 16.4 & -5.74 & 0 \\ -5.74 & 16.4 & 0 \\ 0 & 0 & 0.443 \end{bmatrix} \left\langle \times 10^{-12}\, Pa \right\rangle
$$

$$
\begin{bmatrix} C_{11} & C_{12} & 0 \\ C_{12} & C_{11} & 0 \\ 0 & 0 & C_{66} \end{bmatrix}_{PZT5A}^{ET} = \begin{bmatrix} 69.5 & 24.3 & 0 \\ 24.3 & 69.5 & 0 \\ 0 & 0 & 22.6 \end{bmatrix} \left\langle \times 10^{9}\, Pa \right\rangle
$$

$$
\begin{bmatrix} 0 & 0 & 0 & 0 & d_{15} & 0 \\ 0 & 0 & 0 & d_{15} & 0 & 0 \\ d_{31} & d_{31} & d_{33} & 0 & 0 & 0 \end{bmatrix}_{PZT5A}^{T} = \begin{bmatrix} 0 & 0 & 0 & 0 & 584 & 0 \\ 0 & 0 & 0 & 584 & 0 & 0 \\ -171 & -171 & 374 & 0 & 0 & 0 \end{bmatrix} \left\langle \times 10^{-12} \frac{C}{N} \right\rangle
$$

$$
\begin{bmatrix} \grave{o}_{11} & 0 & 0 \\ 0 & \grave{o}_{11} & 0 \\ 0 & 0 & \grave{o}_{33} \end{bmatrix}_{PZT5A}^{\sigma T} = \begin{bmatrix} 1730 & 0 & 0 \\ 0 & 1730 & 0 \\ 0 & 0 & 1979 \end{bmatrix} \left\langle \grave{o}_{0} \right\rangle
$$

$$
\begin{Bmatrix} \alpha_1 \\ \alpha_2 \\ \alpha_6 \end{Bmatrix}_{PZT5A}^{\sigma E} = \begin{Bmatrix} 1 \\ 1 \\ 0 \end{Bmatrix} \left\langle \times 10^{-6} \frac{1}{K} \right\rangle
$$

$$
\begin{Bmatrix} p_1 \\ p_2 \\ p_3 \end{Bmatrix}_{PZT5A}^{\sigma E} = \begin{Bmatrix} 0.0 \\ 0.0 \\ -200 \end{Bmatrix} \left\langle \times 10^{-6} \frac{C}{m^2 K} \right\rangle \tag{11}
$$

If the assumption that the piezoelectric ceramic composite disk loses contact and loads under open-circuit conditions, then the constant electric displacement stiffness coefficients must be used. The expression and values for the constant electric displacement stiffness values are represented below.

$$\begin{bmatrix} S_{11} & S_{12} & 0 \\ S_{12} & S_{11} & 0 \\ 0 & 0 & S_{66} \end{bmatrix}_{PZT5A}^{DT} = \begin{bmatrix} 14.73 & -7.41 & 0 \\ -7.41 & 14.73 & 0 \\ 0 & 0 & 0.443 \end{bmatrix} \left\langle \times 10^{-12} Pa \right\rangle$$

$$\begin{bmatrix} C_{11} & C_{12} & 0 \\ C_{12} & C_{11} & 0 \\ 0 & 0 & C_{66} \end{bmatrix}_{PZT5A}^{DT} = \begin{bmatrix} 90.9 & 45.7 & 0 \\ 45.7 & 90.9 & 0 \\ 0 & 0 & 22.6 \end{bmatrix} \left\langle \times 10^{9} Pa \right\rangle$$

$$\begin{bmatrix} 0 & 0 & 0 & 0 & g_{15} & 0 \\ 0 & 0 & 0 & g_{15} & 0 & 0 \\ g_{31} & g_{31} & g_{33} & 0 & 0 & 0 \end{bmatrix}_{PZT5A}^{T} = \begin{bmatrix} 0 & 0 & 0 & 0 & 38.13 & 0 \\ 0 & 0 & 0 & 38.13 & 0 & 0 \\ -9.76 & -9.76 & 21.35 & 0 & 0 & 0 \end{bmatrix} \left\langle \times 10^{3} \frac{m^2}{C} \right\rangle$$

$$\begin{Bmatrix} \alpha_1 \\ \alpha_2 \\ \alpha_6 \end{Bmatrix}_{PZT5A}^{\sigma D} = \begin{Bmatrix} -0.9523 \\ -0.9523 \\ 0 \end{Bmatrix} \left\langle \times 10^{-6} \frac{1}{K} \right\rangle \tag{12}$$

Geometry

The composite midpoint is in the PZT5A material as it is thicker than the stainless steel. Therefore, the z_k values are shown in Figure 2 below.

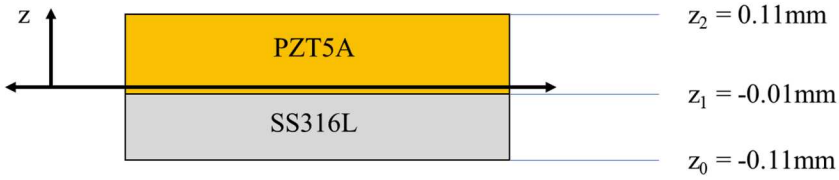

Figure 2. z_k values for composite geometry.

Using the permissible deflection as a benchmark the expected unloaded curvature can be calculated using Equation (13).

$$\Delta w = -\frac{1}{2}\kappa_x \Delta x^2$$

$$\kappa_x = \kappa_y = -2\frac{\Delta w}{\Delta x^2} = 2\frac{0.06\left\langle \times 10^{-3} m \right\rangle}{\left(5.3\left\langle \times 10^{-3} m \right\rangle\right)^2} = 4.272\left\langle \frac{1}{m} \right\rangle \tag{13}$$

Resultants

Using the material properties above the composite's resultant stiffness matrices and thermal force and moment resultants can be calculated as displayed below for both the short- and open-circuit case.

$$\mathbf{A}^E = \begin{bmatrix} 27.99 & 8.62 & 0 \\ 8.62 & 27.99 & 0 \\ 0 & 0 & 9.69 \end{bmatrix} \left\langle \times 10^6 \frac{N}{m} \right\rangle$$

$$\mathbf{B}^E = \begin{bmatrix} -762.2 & -196.0 & 0 \\ -196.0 & -762.2 & 0 \\ 0 & 0 & -283.2 \end{bmatrix} \langle N \rangle$$

$$\mathbf{D}^E = \begin{bmatrix} 0.1180 & 0.0361 & 0 \\ 0.0361 & 0.1180 & 0 \\ 0 & 0 & 0.0410 \end{bmatrix} \langle Nm \rangle$$

$$\mathbf{n}^{Thermal,E} = \begin{Bmatrix} 239.43 \\ 239.43 \\ 0 \end{Bmatrix} \left\langle \frac{N}{mK} \right\rangle$$

$$\mathbf{m}^{Thermal,E} = \begin{Bmatrix} -0.0131 \\ -0.0131 \\ 0 \end{Bmatrix} \left\langle \frac{N}{K} \right\rangle \tag{14}$$

$$\mathbf{A}^D = \begin{bmatrix} 30.56 & 11.18 & 0 \\ 11.18 & 30.56 & 0 \\ 0 & 0 & 9.69 \end{bmatrix} \left\langle \times 10^6 \frac{N}{m} \right\rangle$$

$$\mathbf{B}^D = \begin{bmatrix} -633.92 & -67.72 & 0 \\ -67.72 & -633.92 & 0 \\ 0 & 0 & -283.16 \end{bmatrix} \langle N \rangle$$

$$\mathbf{D}^D = \begin{bmatrix} 0.1275 & 0.0456 & 0 \\ 0.0456 & 0.1275 & 0 \\ 0 & 0 & 0.0410 \end{bmatrix} \langle Nm \rangle$$

$$\mathbf{n}^{Thermal,D} = \begin{Bmatrix} 212.56 \\ 212.56 \\ 0 \end{Bmatrix} \left\langle \frac{N}{mK} \right\rangle$$

$$\mathbf{m}^{Thermal,D} = \begin{Bmatrix} -0.0145 \\ -0.0145 \\ 0 \end{Bmatrix} \left\langle \frac{N}{K} \right\rangle \tag{15}$$

Inverting the ABBD matrix gives the resultant compliance matrix.

$$\mathbf{a}^E = \begin{bmatrix} 0.0487 & -0.0160 & 0 \\ -0.0160 & 0.0487 & 0 \\ 0 & 0 & 0.01294 \end{bmatrix} \left\langle \times 10^{-6} \frac{m}{N} \right\rangle$$

$$\mathbf{b}^E = \begin{bmatrix} 0.3250 & -0.1221 & 0 \\ -0.1221 & 0.3250 & 0 \\ 0 & 0 & -0.8948 \end{bmatrix} \left\langle \times 10^{-3} \frac{1}{N} \right\rangle \tag{16}$$

$$\mathbf{d}^E = \begin{bmatrix} 11.5263 & -3.7720 & 0 \\ -3.7720 & 11.5263 & 0 \\ 0 & 0 & 30.6051 \end{bmatrix} \left\langle \frac{1}{Nm} \right\rangle$$

$$\mathbf{a}^D = \begin{bmatrix} 0.0452 & -0.0195 & 0 \\ -0.0195 & 0.0452 & 0 \\ 0 & 0 & 0.1294 \end{bmatrix} \left\langle \times 10^{-6} \frac{m}{N} \right\rangle$$

$$\mathbf{b}^D = \begin{bmatrix} 0.2757 & -0.1714 & 0 \\ -0.1714 & 0.2757 & 0 \\ 0 & 0 & 0.8948 \end{bmatrix} \left\langle \times 10^{-3} \frac{1}{N} \right\rangle \tag{17}$$

$$\mathbf{d}^D = \begin{bmatrix} 10.7500 & -4.5482 & 0 \\ -4.5482 & 10.7500 & 0 \\ 0 & 0 & 30.6051 \end{bmatrix} \left\langle \frac{1}{Nm} \right\rangle$$

If the composite disk is unloaded and unclamped, the force and moment results at any temperature is zero. Therefore, the only resultants that exist are the thermal expansion resultants. It is therefore possible to compute the effective zero curvature reference temperature T_{ref} (usually the bonding temperature for the composite) using Equation (18).

$$\begin{aligned} T_{ref} &= T_{room} + \Delta T_{ref} \\ \{\boldsymbol{\kappa}\} &= \begin{bmatrix} \mathbf{b} & \mathbf{d} \end{bmatrix} \begin{Bmatrix} \mathbf{n}^{Thermal} \\ \mathbf{m}^{Thermal} \end{Bmatrix} \Delta T_{ref} \\ \begin{Bmatrix} \kappa_x \\ \kappa_y \\ 2\kappa_{xy} \end{Bmatrix} &= \begin{Bmatrix} 4.272 \\ 4.272 \\ 0 \end{Bmatrix} \left\langle \frac{1}{m} \right\rangle \end{aligned} \tag{18}$$

For the closed- and open-circuit case the resulting ΔT_{ref} values to ensure the prescribed curvature at room temperature are shown in Equation (19). It is possible to see here that the effective thermal bending compliance is greater for the open-circuit than the short-circuit due to the stiffer open-circuit PZT.

$$\begin{Bmatrix} 4.272 \\ 4.272 \\ 0 \end{Bmatrix} \left\langle \frac{1}{m} \right\rangle = \begin{Bmatrix} -0.0532 \\ -0.0532 \\ 0 \end{Bmatrix} \left\langle \frac{1}{mK} \right\rangle \Delta T_{ref}^{E}$$
$$\Delta T_{ref}^{E} = -80.31 \langle K \rangle$$
$$\begin{Bmatrix} 4.272 \\ 4.272 \\ 0 \end{Bmatrix} \left\langle \frac{1}{m} \right\rangle = \begin{Bmatrix} -0.0676 \\ -0.0676 \\ 0 \end{Bmatrix} \left\langle \frac{1}{mK} \right\rangle \Delta T_{ref}^{D} \tag{19}$$
$$\Delta T_{ref}^{D} = -63.21 \langle K \rangle$$

The effective ΔT for an applied temperature T_{app} is therefore:

$$\begin{aligned} \Delta T &= \Delta T_{app} + \Delta T_{ref} \\ \Delta T_{app} &= T_{app} - T_{room} \\ \Delta T &= T_{app} - T_{ref} \end{aligned} \tag{20}$$

Center-Edge Deflection vs Temperature

Using T_{ref} calibrated to the center-edge deflection of 0.06mm at room temperature ($\Delta T_{app} = 0$). The expression for center-edge deflection Δw of the short- and open-circuit disks as a function of temperature can be calculated as shown in Equation (21) and is plotted in Figure 3. The deflection response to temperature of the open-circuit composite is approximately 2.4% greater than the short-circuit composite.

$$\begin{Bmatrix} \kappa_x \\ \kappa_y \\ 2\kappa_{xy} \end{Bmatrix} = \begin{bmatrix} \mathbf{b} & \mathbf{d} \end{bmatrix} \begin{Bmatrix} \mathbf{n}^{Thermal} \\ \mathbf{m}^{Thermal} \end{Bmatrix} \left[\Delta T_{app} + \Delta T_{ref} \right]$$
$$\Delta w = \frac{1}{2} \kappa_x \left[5.3 \times 10^{-3} m \right]^2$$
$$\Delta w^{E} = \left[-7.4712 \left\langle \times 10^{-7} \frac{m}{K} \right\rangle \right] \Delta T_{app}^{E} \tag{21}$$
$$\Delta w^{D} = \left[-9.4923 \left\langle \times 10^{-7} \frac{m}{K} \right\rangle \right] \Delta T_{app}^{E}$$

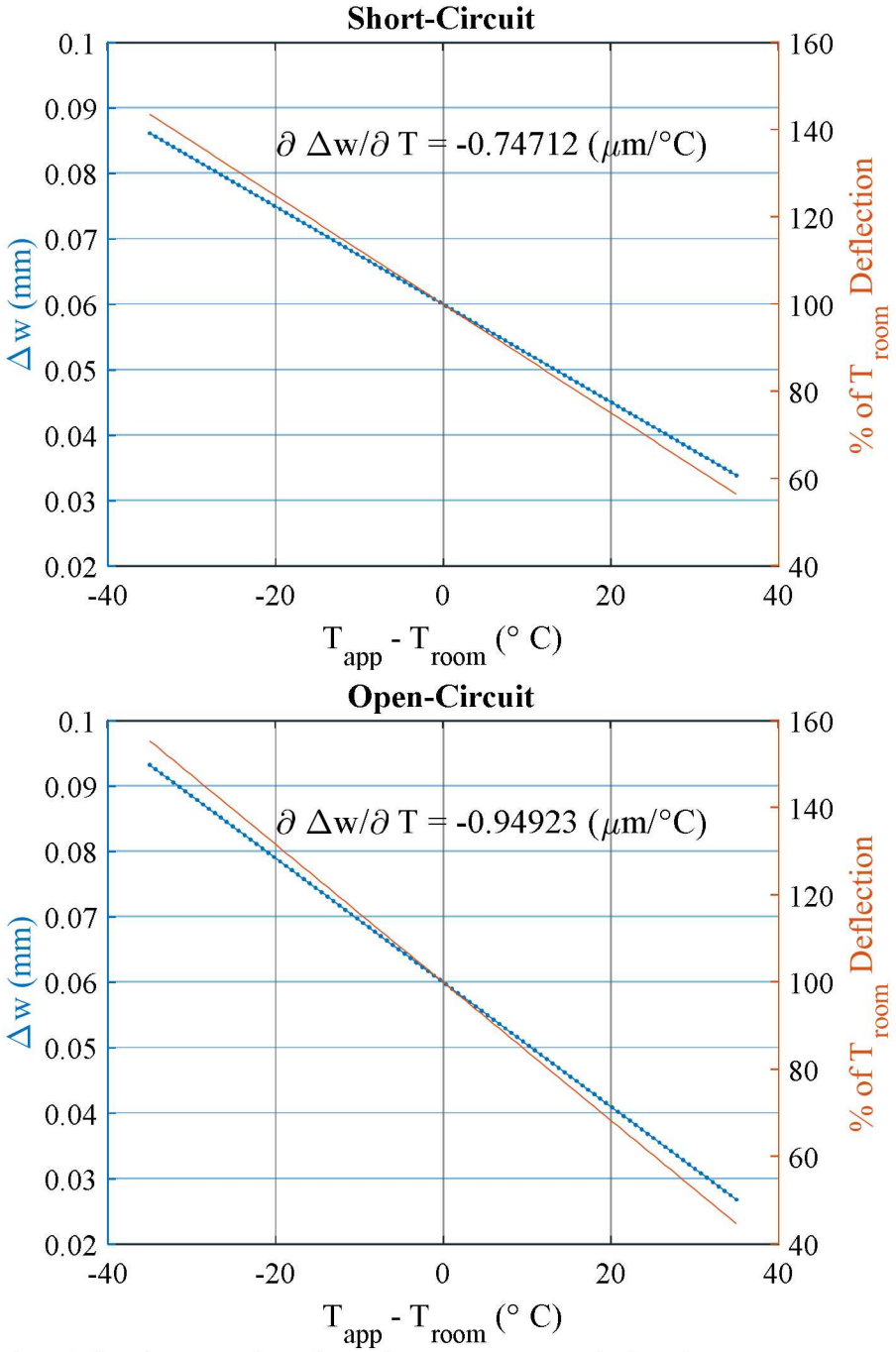

Figure 3. Edge deflection as a function of temperature variation from room temp.

The stainless-steel has significantly greater the thermal expansion coefficient than the PZT5A. Therefore, increases in temperature will reduce the curvature of the composite disk. The change in curvature from the rest state curvature to the flat ("pressed") state will be less and the electromechanical response will decrease correspondingly. Conversely, a temperature decrease will increase the rest state curvature and increase the electromechanical responsiveness.

Voltage Buildup vs Temperature

In the event of the piezoelectric composite disk breaking contact with a dissipative circuit, the temperature induced flexing and resulting stress change in the PZT5A layer will cause the open-circuit system to build up a voltage due to the charge released from the 3-1 excitation mode piezoelectric effect. The open-circuit voltage can be calculated using Equation (3) and for the poling direction electric field, the expression can be rewritten as shown in Equation (22).

$$E_z^{OC} = -\frac{1}{\delta_{33}^{\sigma T}}\left[d_{31}^T \left[\sigma_x + \sigma_y \right] + d_{33}^T \sigma_z + p_3^{\sigma E} \Delta T \right]$$

if:

$$\sigma_z = \tau_{yz} = \tau_{xz} = \tau_{xy} = 0,\ \sigma_x = \sigma_y$$

$$E_z^{OC} = -\frac{1}{\delta_{33}^{\sigma T}}\left[2 d_{31}^T \sigma_x + p_3^{\sigma E} \Delta T \right] \tag{22}$$

$$V^{OC} = -E_z^{OC}(z_2 - z_1) = -2.3427 \left\langle \times 10^{-6} \frac{V}{Pa} \right\rangle \sigma_x - 1.37 \left\langle \frac{V}{K} \right\rangle \Delta T$$

$$Q^{OC} = V^{OC} C_{PZT} = -2.1757 \left\langle \times 10^{-14} \frac{C}{Pa} \right\rangle \sigma_x - 1.2723 \left\langle \times 10^{-8} \frac{C}{K} \right\rangle \Delta T$$

The average in plane stress of the PZT5A layer depends on whether the composite disk is free to bend or clamped. If the disk is free to bend, the PZT layer in-plane stress expression is:

$$\begin{Bmatrix} \mathbf{N} \\ \mathbf{M} \end{Bmatrix} = \begin{Bmatrix} \mathbf{0} \\ \mathbf{0} \end{Bmatrix} \tag{23}$$

$$
\begin{aligned}
\begin{Bmatrix} \overline{\sigma}_x \\ \overline{\sigma}_y \\ \overline{\tau}_{xy} \end{Bmatrix}_{PZT5A}^{D,unclamped} &= \frac{1}{z_2 - z_1} \int_{z_1}^{z_2} \begin{Bmatrix} \sigma_x \\ \sigma_y \\ \tau_{xy} \end{Bmatrix} dz \\
&= \frac{1}{z_2 - z_1} \int_{z_1}^{z_2} \begin{bmatrix} C_{11} & C_{12} & 0 \\ C_{12} & C_{11} & 0 \\ 0 & 0 & C_{66} \end{bmatrix}_{PZT5A}^{D} \left[\begin{Bmatrix} \varepsilon_x^0 \\ \varepsilon_y^0 \\ \gamma_{xy}^0 \end{Bmatrix} + z \begin{Bmatrix} \kappa_x \\ \kappa_y \\ 2\kappa_{xy} \end{Bmatrix} - \begin{Bmatrix} \alpha_x \\ \alpha_y \\ \alpha_{xy} \end{Bmatrix}_{PZT5A}^{D} \Delta T \right] dz \\
&= \frac{1}{z_2 - z_1} \int_{z_1}^{z_2} \begin{bmatrix} C_{11} & C_{12} & 0 \\ C_{12} & C_{11} & 0 \\ 0 & 0 & C_{66} \end{bmatrix}_{PZT5A}^{D} \left[\left(\begin{bmatrix} \mathbf{a} & \mathbf{b} \end{bmatrix} + z \begin{bmatrix} \mathbf{b} & \mathbf{d} \end{bmatrix} \right) \begin{Bmatrix} \mathbf{n}^{Thermal} \\ \mathbf{m}^{Thermal} \end{Bmatrix} \Delta T - \begin{Bmatrix} \alpha_x \\ \alpha_y \\ \alpha_{xy} \end{Bmatrix}_{PZT5A}^{D} \Delta T \right] dz \\
&= \frac{\Delta T}{z_2 - z_1} \begin{bmatrix} C_{11} & C_{12} & 0 \\ C_{12} & C_{11} & 0 \\ 0 & 0 & C_{66} \end{bmatrix}_{PZT5A}^{D} \left[\begin{bmatrix} \left(\begin{bmatrix} \mathbf{a} & \mathbf{b} \end{bmatrix} \right) \begin{Bmatrix} \mathbf{n}^{Thermal} \\ \mathbf{m}^{Thermal} \end{Bmatrix}_{PZT5A}^{D} - \begin{Bmatrix} \alpha_x \\ \alpha_y \\ \alpha_{xy} \end{Bmatrix}_{PZT5A}^{D} \end{bmatrix} \left[z_2 - z_1 \right] \right. \\
&\qquad \left. + \begin{bmatrix} \mathbf{b} & \mathbf{d} \end{bmatrix} \begin{Bmatrix} \mathbf{n}^{Thermal} \\ \mathbf{m}^{Thermal} \end{Bmatrix}_{PZT5A}^{D} \frac{1}{2} \left[z_2^2 - z_1^2 \right] \right] \\
\begin{Bmatrix} \overline{\sigma}_x \\ \overline{\sigma}_y \\ \overline{\tau}_{xy} \end{Bmatrix}_{PZT5A}^{D,unclamped} &= \Delta T \begin{Bmatrix} 0.20887 \\ 0.20887 \\ 0 \end{Bmatrix} \left\langle \times 10^6 \frac{Pa}{K} \right\rangle
\end{aligned}
$$

(24)

If the disk is clamped from bending, the PZT layer in-plane strain and stress expressions are:

$$\{\boldsymbol{\kappa}\} = \{\mathbf{N}\} = \{\mathbf{0}\}$$

$$\{\mathbf{0}\} = \begin{bmatrix}\mathbf{b} & \mathbf{d}\end{bmatrix} \underbrace{\left[\begin{Bmatrix} \mathbf{0} \\ \mathbf{M} \end{Bmatrix} + \begin{Bmatrix} \mathbf{n}^{Thermal} \\ \mathbf{m}^{Thermal} \end{Bmatrix} \Delta T \right]}_{\begin{Bmatrix} \bar{\mathbf{N}} \\ \bar{\mathbf{M}} \end{Bmatrix}}$$

$$\bar{M}_x = \bar{M}_y$$

$$\bar{N}_x = \bar{N}_y = \bar{N}_{xy} = \bar{M}_{xy} = 0$$

$$M_x = \left[m_x^{Thermal} - \frac{b_{11} + b_{12}}{d_{11} + d_{12}} n_x^{Thermal} \right] \Delta T$$

$$\left\{\boldsymbol{\varepsilon}^0\right\} = \begin{bmatrix}\mathbf{a} & \mathbf{b}\end{bmatrix} \begin{Bmatrix} \mathbf{n}^{Thermal} \\ \mathbf{m}^{Thermal} + \begin{Bmatrix} m_x^{Thermal} - \dfrac{b_{11} + b_{12}}{d_{11} + d_{12}} n_x^{Thermal} \\ m_x^{Thermal} - \dfrac{b_{11} + b_{12}}{d_{11} + d_{12}} n_x^{Thermal} \\ 0 \end{Bmatrix} \end{Bmatrix} \Delta T \tag{25}$$

$$
\begin{aligned}
\begin{Bmatrix} \bar{\sigma}_x \\ \bar{\sigma}_y \\ \bar{\tau}_{xy} \end{Bmatrix}_{PZT5A}^{D,clamped} &= \frac{1}{z_2 - z_1} \int_{z_1}^{z_2} \begin{Bmatrix} \sigma_x \\ \sigma_y \\ \tau_{xy} \end{Bmatrix} dz \\
&= \frac{1}{z_2 - z_1} \int_{z_1}^{z_2} \begin{bmatrix} C_{11} & C_{12} & 0 \\ C_{12} & C_{11} & 0 \\ 0 & 0 & C_{66} \end{bmatrix}_{PZT5A}^{D} \left[\begin{Bmatrix} \varepsilon_x^0 \\ \varepsilon_y^0 \\ \gamma_{xy}^0 \end{Bmatrix} - \begin{Bmatrix} \alpha_x \\ \alpha_y \\ \alpha_{xy} \end{Bmatrix}_{PZT5A}^{D} \Delta T \right] dz \\
&= \frac{1}{z_2 - z_1} \int_{z_1}^{z_2} \begin{bmatrix} C_{11} & C_{12} & 0 \\ C_{12} & C_{11} & 0 \\ 0 & 0 & C_{66} \end{bmatrix}_{PZT5A}^{D} \left[\begin{bmatrix} \mathbf{a} & \mathbf{b} \end{bmatrix} \begin{Bmatrix} \mathbf{n}^{Thermal} \\ \mathbf{m}^{Thermal} + \begin{Bmatrix} m_x^{Thermal} - \dfrac{b_{11} + b_{12}}{d_{11} + d_{12}} n_x^{Thermal} \\ m_x^{Thermal} - \dfrac{b_{11} + b_{12}}{d_{11} + d_{12}} n_x^{Thermal} \\ 0 \end{Bmatrix} \end{Bmatrix} - \begin{Bmatrix} \alpha_x \\ \alpha_y \\ \alpha_{xy} \end{Bmatrix}_{PZT5A}^{D} \right] \Delta T dz \\
\begin{Bmatrix} \bar{\sigma}_x \\ \bar{\sigma}_y \\ \bar{\tau}_{xy} \end{Bmatrix}_{PZT5A}^{D,unclamped} &= \Delta T \begin{Bmatrix} 0.67017 \\ 0.67017 \\ 0 \end{Bmatrix} \left\langle \times 10^6 \frac{Pa}{K} \right\rangle
\end{aligned}
\tag{26}
$$

The combination of Equations (22) and (24) gives the open-circuit voltage buildup of the piezoelectric composite disk as shown in Equation (27) and Figure 4.

$$
\begin{aligned}
V^{Open,unclamped} &= -1.8593 \left\langle \frac{V}{K} \right\rangle \Delta T \\
V^{Open,clamped} &= -2.9400 \left\langle \frac{V}{K} \right\rangle \Delta T \\
Q^{Open,unclamped} &= -1.7268 \left\langle \times 10^{-8} \frac{C}{K} \right\rangle \Delta T \\
Q^{Open,clamped} &= -2.7304 \left\langle \times 10^{-8} \frac{C}{K} \right\rangle \Delta T
\end{aligned}
\tag{27}
$$

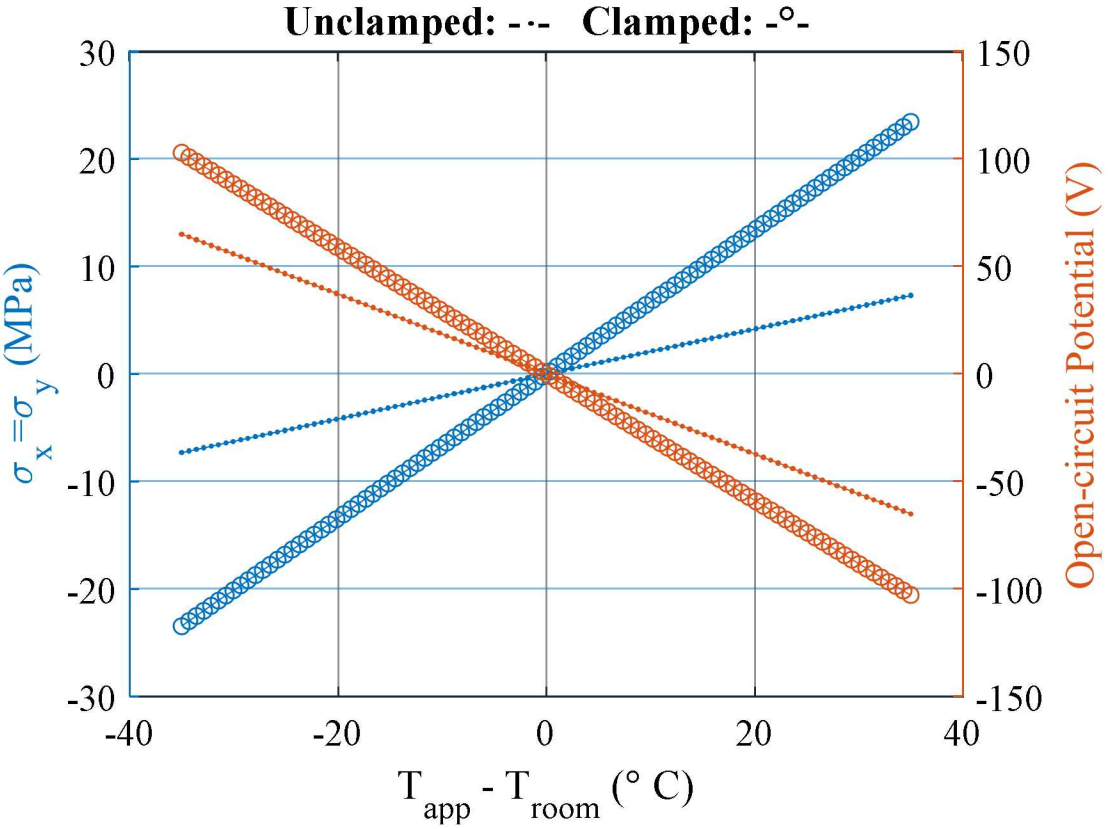

Figure 4. In plane stress in the PZT5A layer and resulting open-circuit voltage from the 3-1 mode piezoelectric excitation.

EXPERIMENTAL VERIFICATION

Dilatometer Measurements

Open-circuit thermal expansion induced edge deflection was measured using a NETZSCH GmbH DIL 402 Expedis Select dilatometer. A piezoelectric composite disk was held in place by a push rod, centered on the disk, and pressed against a blacking block. This configuration as shown in Figure 5. The specimen was cooled from room temperature of 21˚C to -15˚C, then heated to 55˚C, then cooled to 28˚C all at the rate of 1K/min. This procedure was performed on two separate composite disk specimens.

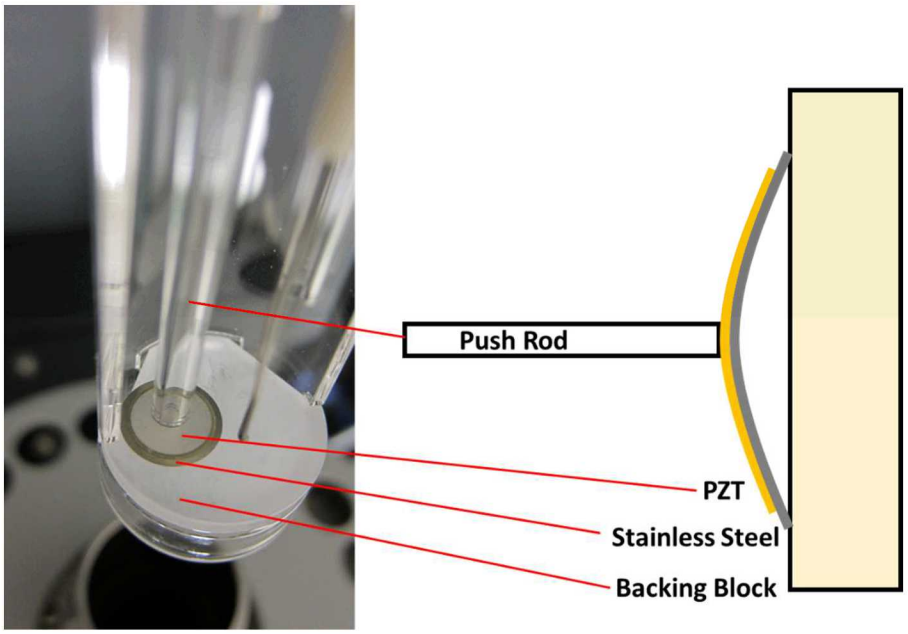

Figure 5. Dilatometer set up of edge deflection in a piezoelectric composite disk.

The results of the edge deflection measurements relative to the deflection at room temperature as measured by the dilatometer is shown in Figure 6. The predicted edge deflection values calculated from the open-circuit (OC) and short-circuit (SC) model expressions in Equation (21) are also plotted.

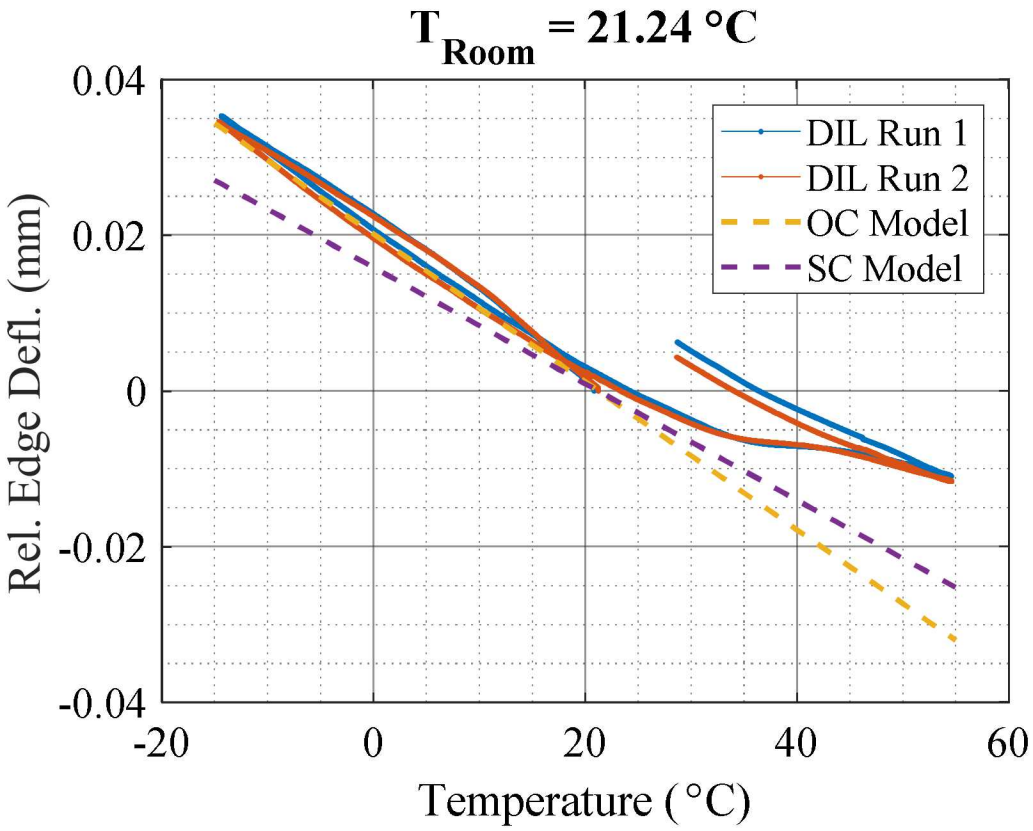

Figure 6. Dilatometer relative edge deflection measurements of two composite disk specimens as compared to the open-circuit (OC) and short-circuit (SC) model predictions.

It can be seen from Figure 6, that there is good agreement in the edge deflection values between the measured and predicted models. However, upon heating, the measured edge deflection becomes highly nonlinear and hysteretic while following the predicted slope upon cooling again. The cause for this nonlinearity and hysteresis could be hypothesized as specimen reaching full flatness at around 35˚C and having an initial room temperature edge deflection of much less than 0.06mm.

Pyroelectric Measurements

Effective short-circuit pyroelectric measurements of the complete composite disk were measured. Composite disk specimens were thermally loaded in an environmental chamber that was electrically heated and liquid nitrogen cooled. Pyroelectric current was measured using a Keithley Model 6487 picoammeter. The piezoelectric composite disks are held in a spring-loaded fixture which puts the loading conditions in between a clamped and unclamped mode.

The effective short-circuit pyroelectric measurement of the composite includes both the inherent pyroelectric response of the PZT material as well as the thermal flex induced piezoelectric response. The lowpass filtered current and thermal loading rates for two heating and cooling cycles are shown in Figures 7 and 8 below. The effective short-circuit pyroelectric current is shown to have good linear agreement with the temperature loading rate across the entire temperature loading range. This shows that the PZT material and composite does not undergo nonlinear behavior. The effective pyroelectric and (pyro-coulombic) coefficients are much greater than that predicted in Equation (27). This indicates that either the pyroelectric coefficient is much greater in the PZT layer than that of the reference values or the piezoelectric and elastic coefficients of the PZT layer are greater than the reference values. Using the short-circuit current as an estimate for the open-circuit bound charge on the PZT layer, the pyro-voltaic relation for the composite disks can be estimated to be 3.855V/K.

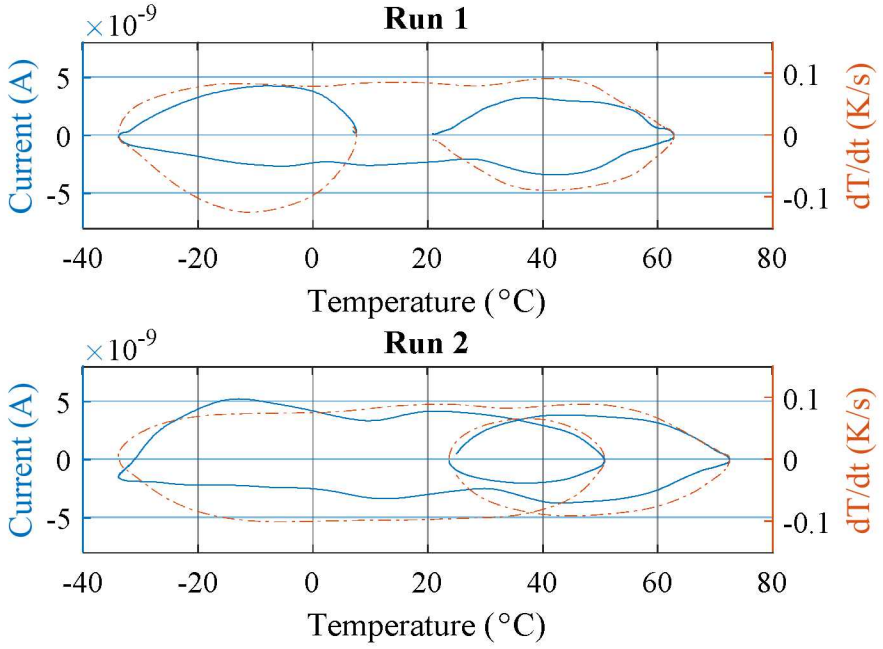

Figure 7. Effective pyroelectric current and Temperature loading rates from -30 to 70 Celsius.

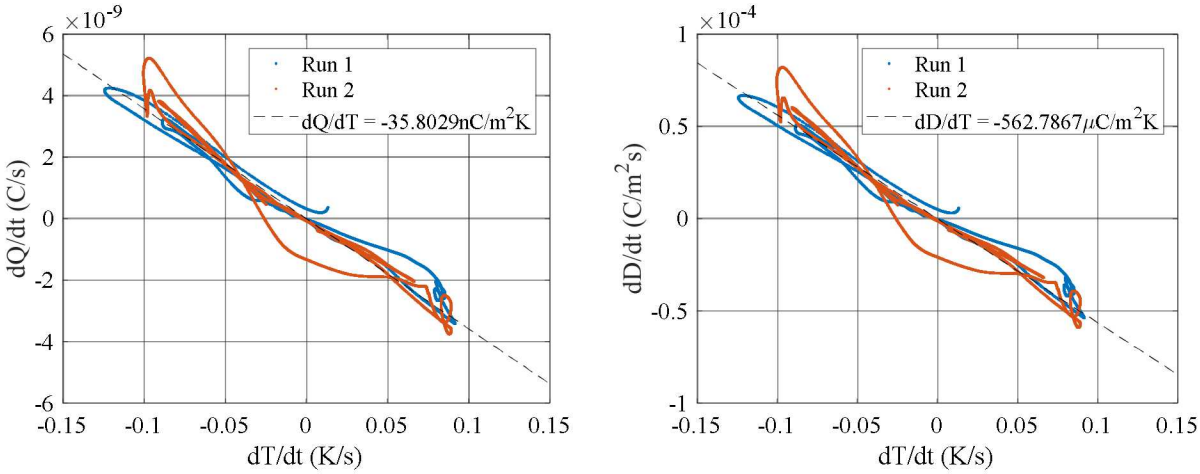

Figure 8. a) Effective pyroelectric current and b) Electric displacement rate as a function of temperature loading rate.

CONCLUSION

At a fixed temperature, the piezoelectric potential generated by changing or removing the curvature of the composite disk as it is pushed down from the top. This flex creates an in-plane compression stress in the PZT layer and activates the 3-1 mode piezoelectric coupling effect.

The unloaded flex of the composite disk is a result of the thermal expansion difference between thermal expansion strains between the PZT and stainless-steel layers in addition to strains introduced during manufacturing. The stainless-steel layer has a significantly higher thermal expansion coefficient than the PZT layer. Therefore, as temperatures increase the curvature of the composite disk decreases. At elevated temperatures, the natural curvature of the disk disappears as can be seen in Figure 6 where above 35 degrees Celsius the change in edge deflection of the disk significantly decreases to changes in temperature. The loss in the composite disk curvature prevents electromechanical response as there is less or no flex from pressing on the disk. One possible solution to increasing the operating temperature range of the composite disk is to introduce higher built in curvature.

The effective pyroelectric response of the entire composite disk appears to be a combination of both the pyroelectric properties of the PZT layer and the flex induced piezoelectric response from thermal expansion differences. This can be seen in the voltage and charge production expressions in Equations (22) and (27) although the measured effective pyroelectric coefficient is greater and indicates inaccuracies in the reference material properties. Equation (21) shows that temperature dependence of the curvature is significantly greater for the open-circuit than the short-circuit scenario. This can be explained in Figure 9, which shows that in the open-circuit scenario, the pyroelectric effect creates an electric field in the PZT that causes the piezoelectric effect to create negative strains in-plane. This behavior is shown in Equation (12) where the open-circuit in-plane thermal expansion coefficients are negative. Smaller thermal expansions in the PZT layer create larger incompatibilities between the PZT and stainless-steel layers leading to higher curvature dependence on temperature and greater curvatures at lower temperatures.

Significant curvatures in the composite can lead to higher occurrences in loss of electrical contact, higher sensitivity of the composite disk and in turn false positive key presses from pressure applied to neighbors, and loss electrical contact can cause electrical discharge as the open-circuit voltage-temperature relation is non-trivial.

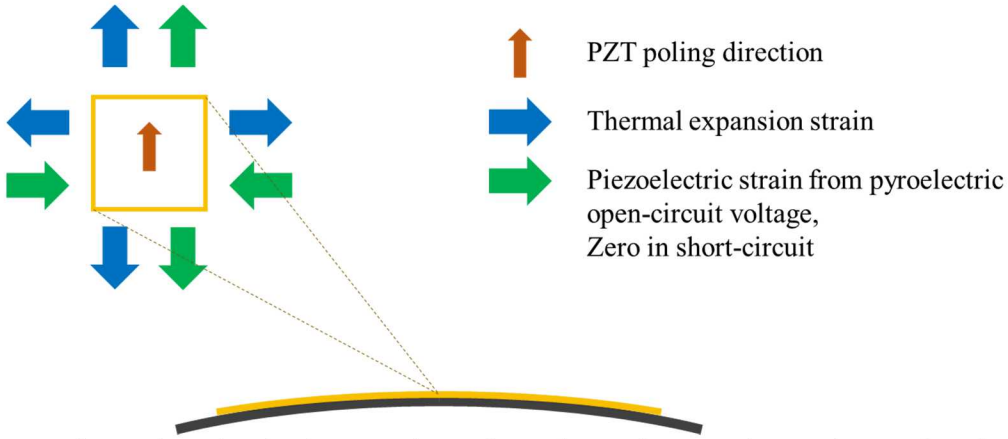

Figure 9. Thermal strains in the PZT layer from thermal expansion and pyroelectric open-circuit piezoelectric effect for positive temperature fluctuations. The in-plane strain is greater